ARCHIVES
of
FOUNDRY ENGINEERING

ISSN (2299-2944)
Volume 2026
Issue 3/2026

61 – 70

8/3

10.24425/afe.2026.158019

Published quarterly as the organ of the Foundry Commission of the Polish Academy of Sciences

Industrial Potential of Additively Manufactured H13 Steel Components: A Service Life Study

M. Pinta [a, b, *], L. Socha [a], L. Kučerová [b], M. Dvořák [c]

[a] Department of Applied Technologies and Materials Research, Institute of Technology and Business in České Budějovice, Okružní 517/10, 370 01 České Budějovice, Czech Republic

[b] Department of Materials and Engineering Metallurgy, Faculty of Mechanical Engineering, University of West Bohemia, Univerzitní 2732/8, 301 00 Plzeň, Czech Republic

[c] MOTOR JIKOV Fostron a.s., Mold Division, Kněžskodvorská 2277, 370 04 České Budějovice, Czech Republic

* Corresponding author: E-mail address: 22038@vste.cz

Received 26.05.26; accepted in revised form 18.08.26; available online 23.09.2026

Abstract

This article focuses on evaluating the service life of components made from H13 tool steel manufactured using additive manufacturing, specifically 3D printing. This was done by comparing them with components produced by conventional manufacturing methods. H13 tool steel is widely used due to its high mechanical strength and resistance to thermal cycling, properties which are particularly important in high-pressure die casting (HPDC) applications. In such processes, components are regularly subjected to significant mechanical and thermal stresses. The article provides a comprehensive comparison of dimensional stability, porosity, surface roughness, hardness, and operational wear in conventionally and additively manufactured H13 components. Additional measurements of surface roughness were conducted to provide further insight into the material's surface condition and the overall reliability of the additively manufactured components. The results provide insight into the advantages and limitations of additively manufactured H13 components and support their potential industrial application in high-pressure die casting.

Keywords: Operational life, High-pressure die casting, Tool steel, H13, 3D printing

1. Introduction

In its as-built state, H13 tool steel produced by laser powder bed fusion (LPBF) exhibits a fine martensitic matrix with a submicrostructure and a proportion of residual austenite [1,2]. This microstructure results in high strength and hardness, with a yield strength typically ranging from 1300 to 1600 MPa and a tensile strength of approximately 1700–1900 MPa [1,3]. Studies report that with optimised process parameters, especially with higher laser power and corresponding scanning speed, a relative density exceeding 99.5% can be achieved [3,4]. However, the specific combination of parameters varies significantly between individual studies, which limits the possibility of comparing them directly and complicates the practical application of these findings in industrial production [5].

A significant advantage of additive manufacturing, particularly laser- and electron beam-based processes, is its ability to produce geometrically complex structures, such as aerospace components, conformal cooling channels, and overhanging features, which are difficult to manufacture using conventional technologies [6–10].

© The Author(s) 2026. Open Access. This article is licensed under a Creative Commons Attribution 4.0 International License (http://creativecommons.org/licenses/by/4.0/), which permits use, sharing, adaptation, distribution and reproduction in any medium or format, as long as you give appropriate credit to the original author(s) and the source, provide a link to the Creative Commons licence, and indicate if changes were made.

However, these geometries place increased demands on the stability of the process and the accuracy of the construction parameter settings, particularly in terms of energy density control and heat dissipation during melting [11]. The scanning strategy, energy density, and construction orientation fundamentally influence the occurrence of internal defects, dimensional accuracy, and the resulting mechanical properties [12–14]. For instance, insufficient energy density can lead to insufficient layer fusion and increased porosity, while excessive heat input promotes the formation of cracks and residual stresses [13]. Most published studies evaluate material characteristics primarily on simple test bodies [14], while the production of functionally complex channel structures from H13 steel remains less systematically explored [15].

In addition to the parameters of the structure itself, subsequent heat treatment also plays a key role, as it reduces residual stresses and stabilises the microstructure [15]. After quenching and tempering, LPBF H13 steel achieves a hardness of approximately 45–55 HRC, depending on the selected mode [16]. Lower tempering temperatures, typically around 500–550 °C, lead to higher strength and hardness, while higher temperatures in the range of approximately 550–650 °C promote increased toughness and a partial reduction in internal stress [16,17]. However, published research often focuses only on limited ranges of thermal regimes and often does not link printing parameters with the resulting microstructure and mechanical or fatigue behaviour of the material [18].

The fatigue life of LPBF H13 steel is significantly influenced by surface quality, the presence of printing defects, and structure orientation [16,19]. By minimising defects and with appropriate surface treatments, the fatigue limit can reach values exceeding approximately 600 MPa, which is comparable to conventionally manufactured steel [16,20]. Surface treatments and post-processing can further improve tribological properties and resistance to wear [21–25]. Nevertheless, there is still limited information on which specific combinations of process and post-process parameters lead to reproducibly high fatigue resistance, especially for components with complex geometry [26].

H13 material produced using LPBF has considerable potential for applications particularly in the manufacture of injection moulds and hot working tools, where a combination of high strength, thermal stability, and resistance to thermal stress is required [27]. The relative density of manufactured parts commonly exceeds 99%, and tensile strength can reach up to approximately 2000 MPa after the optimisation of the process [27]. However, challenges persist in stabilising the mechanical properties, limiting anisotropy, and minimising residual stresses [28]. Although the additive manufacturing of this material has been intensively studied in recent years [29], the relationship between process parameters, subsequent heat treatment, and the resulting mechanical properties has not yet been described in sufficient depth [30].

This means that the H13 material produced using LPBF has considerable potential for application in the field of injection moulds. However, persistent problems must be taken into account, primarily in stabilising mechanical properties, removing residual stresses, and limiting process defects that can negatively affect tool life [31]. In recent years, additive manufacturing using laser powder bed fusion (SLM/LPBF) has proven to be a promising avenue for the production of tools from H13 steel, a material which is already commonly used for applications requiring high strength and heat resistance [31].

2. Material and methods

The components analysed in this article were manufactured in cooperation with MOTOR JIKOV Fostron a.s. and academic institutions including the University of West Bohemia in Pilsen, the Technical University of Liberec, and the Institute of Technology and Business in České Budějovice. The design and production were carried out using selective laser melting (SLM) additive technology in cooperation between MOTOR JIKOV Fostron a.s. and the Technical University of Liberec. The experimental evaluation of the dimensional accuracy of the manufactured components, which is the main focus of this article, was subsequently conducted at the Institute of Technology and Business in České Budějovice. The experimental procedures and characterisation methods used are described in detail in the following sections.

2.1. Testing methods

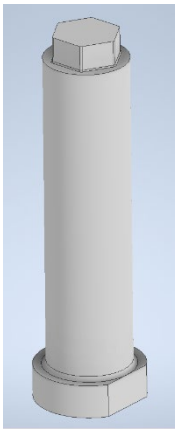
The manufactured components were operationally verified in the MOTOR JIKOV Slévárna a.s. pressure foundry. The components were integrated into a mould designed for pressure casting of aluminium alloys in order to assess their behaviour under real production loads. The expected service life was set at approximately 120,000 casting cycles.

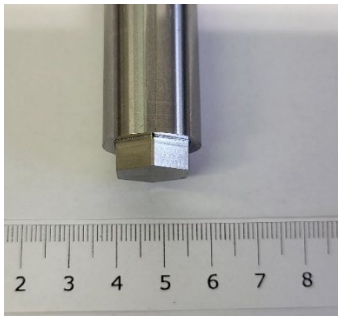
The experimental operation ran on Colosio PFO1000 pressure casting machines, which have a closing force of up to 9,810 kN and a maximum injection force of 738 kN. During and after deployment, the components were subjected to a series of analyses to assess their operational condition and degradation mechanisms, as follows:

- Scanning
- Roughness measurement on a confocal light microscope
- Vickers hardness measurement

2.2 Analysed components and samples

Figure 1a shows the complete component from which test samples were taken for the evaluation of mechanical properties. Samples were prepared from both conventionally manufactured and additively manufactured components for comparative analysis. The testing was carried out on the functional part of the component, which has a hexagonal geometry and is directly exposed to molten metal during operation. Figures 1a and 1b show the component geometry, which is identical for both conventionally and additively manufactured variants.





a) whole component b) detail of working part

Fig. 1. Geometry of the component used for both conventionally and additively manufactured variants

Conventionally and additively manufactured components were made from AISI H13 tool steel (W.nr. 1.2344), which is commonly used for hot work tools. This material is characterised by high strength at elevated temperatures, good resistance to thermal stress and thermally induced fatigue, as well as a favourable combination of toughness and ductility. These properties mean that H13 is considered the standard material for applications exposed to cyclic thermal and mechanical stresses.

The nominal chemical composition of the supplied material, as declared by the manufacturer, is shown in Table 1.

Table 1.
Comparison of the chemical composition of material H13

	C [%]	Cr [%]	Si [%]	Mo [%]	V [%]	Mn [%]
H13-attestation	0.3-0.45	4.7-5.5	0.8-1.2	1.3-1.7	0.8-1.2	0.2-0.5
H13 – measured	0.388	5.079	1.067	1.650	1.101	0.334

The components were produced using two different manufacturing routes. The conventional components were manufactured from solid H13 steel stock using conventional machining, particularly turning and milling, whereas the additive components were produced from H13 metal powder using selective laser melting (SLM). Both component types subsequently underwent identical heat treatment, final machining, and coating procedures.

The additive components were manufactured using the SLM method, in which individual layers of metal powder are gradually melted and bonded together using a laser beam. The basic parameters of the SLM process are shown in Table 2.

Table 2.
SLM process parameters

Layer height	40	µm
Laser power	350	W
Scanning speed	1216	mm/s
Hatch spacing	0.12	mm

During additive manufacturing using selective laser melting, internal stresses arise due to high heating and cooling rates. In order to minimise these stresses, stabilise the microstructure, and achieve the desired hardness (46 ± 2 HRC) and heat resistance, heat treatment was performed after the completion of 3D printing.

Heat treatment was applied using the same procedure to both conventionally and additively manufactured components. The process included homogenisation annealing at a temperature of 1080 °C with a holding time of 60 min, followed by two-stage preheating at temperatures of 650 °C and 850 °C, each with a holding time of 15 min. Austenitisation took place at a temperature of 1030 °C for 30 minutes, with a cooling rate of 28 °C·min^{-1}. This was followed by triple tempering at temperatures of 570 °C, 590 °C, and 555 °C, each with a holding time of 3 hours. The resulting hardness after the sequence of homogenisation annealing, quenching, and tempering reached values of 46–47 HRC (460–470 HV).

The final dimensions of the components were achieved using the conventional machining operations of turning and milling. In the final stage of production, an ALWIN® (CrAlSiN) nanocomposite PVD coating was applied to the functional surfaces, which exhibits high resistance to molten metal adhesion and thermal stability exceeding 1000 °C. These properties make it ideal for use on tools designed for high-pressure aluminium alloy casting.

All four components had the same geometry and were installed simultaneously at four different positions in the die-casting mould as shown in Figure 2. Thus, C-3 and C-4, as well as 3D-3 and 3D-4, differed in their positions within the mould. The designation C refers to conventional manufacturing, whereas 3D refers to SLM additive manufacturing. All components were made of H13 tool steel and had identical geometry and subsequent heat treatment, machining, and coating procedures. The conventionally manufactured components C-3 and C-4 were located in the upper-right and lower-right positions, respectively, whereas the additively manufactured components 3D-3 and 3D-4 were located in the upper-left and lower-left positions, respectively, as viewed in Figure 2.

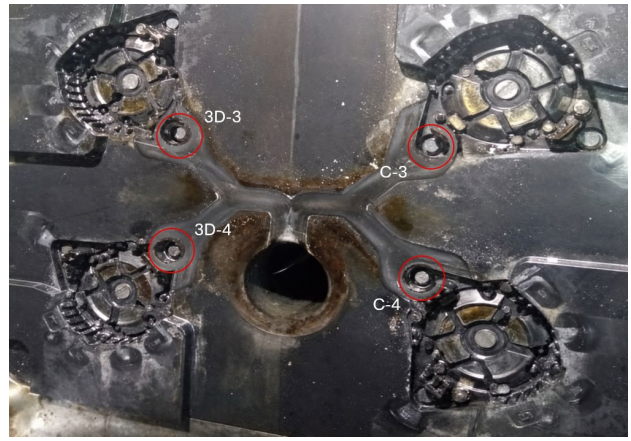


Fig. 2. Positions of the conventionally manufactured components C-3 and C-4 and the additively manufactured components 3D-3 and 3D-4 in the die-casting mould

Four components were selected for testing mechanical properties, as shown in Table 3.

Table 3.
Description of the components selected for testing mechanical properties

Samples	Manufacturing method	Operational exposure
C-3	Conventional	115,500 cycles
C-4	Conventional	115,500 cycles
3D-3	SLM	115,500 cycles
3D-4	SLM	115,500 cycles

The primary purpose of the testing was to compare the properties of conventionally and additively manufactured components. For this purpose, two conventionally manufactured components designated C-3 and C-4 and two additively manufactured components designated 3D-3 and 3D-4 were selected. The components were subjected to operational testing and were deployed in a pressure casting mould. The components were deployed in the mould for 115,500 casting cycles, which is almost the limit of their service life. The operational testing was conducted at the high-pressure die-casting foundry of MOTOR JIKOV Slévárna a.s. and lasted approximately one year under normal foundry operating conditions.

Representative photographs of the conventionally and additively manufactured components before and after operational testing are shown in Figures 3 and 4 a, b, c, d.



a) component C-3 before operational testing *b) component C-3 after operational testing* *c) component C-4 before operational testing* *d) component C-4 after operational testing*

Fig. 3. Components C-3 and C-4 before and after operational testing



a) component 3D-3 before operational testing *b) component 3D-3 after operational testing* *c) component 3D-4 before operational testing* *d) component 3D-4 after operational testing*

Fig. 4. Components 3D-3 and 3D-4 before and after operational testing

3. Results and discussion

Scanning of conventional component C-3

Figure 5 shows the results of 3D scanning of component C-3 in the individual stages of processing and subsequent operational loading. The colour scale indicates surface deviations, with blue shades representing minimal differences and red tones representing maximum deviations. In the first step, i.e., in the as-manufactured condition, the surface of the conventionally manufactured component was significantly uneven, with numerous deviations indicated by the purple areas. After heat treatment, more significant dimensional changes appear, which are particularly evident in the areas shown in purple. Machining largely eliminates these differences and the surface becomes uniform, as evidenced by the predominance of green tones. Coating further evens out the surface, and the resulting structure shows only minimal deviations. After 16,000 cycles, the surface remains stable and the changes are only local in character.

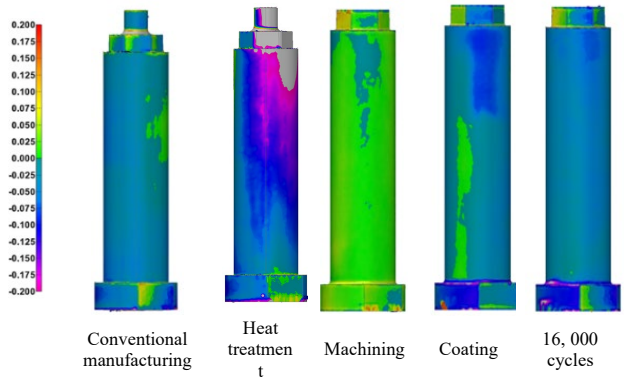


Fig. 5. First part of the technological process of component C-3

Figure 6 shows the results of 3D scanning of the surface of component C-3 after various numbers of operating cycles.

After 32,000 cycles, the surface is still relatively homogeneous with minor local changes. After 78,000 cycles, more significant deviations begin to appear, indicating a slight loss of material. At 97,000 cycles, these changes spread further and the surface becomes less uniform. After 103,400 cycles, more extensive areas with greater deviations are visible, indicating gradual surface wear. After reaching 115,500 cycles, surface degradation is already apparent over a larger area, which confirms gradual deterioration of surface properties under long-term loading.

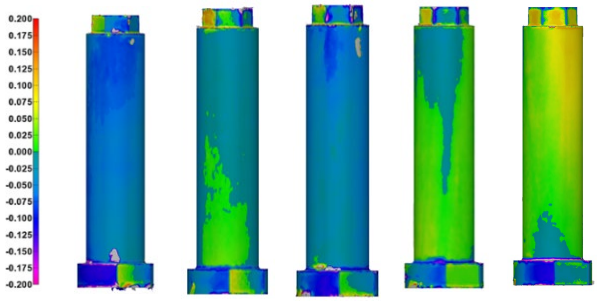


Fig. 6. Second part of the technological process of component C-3

Scanning of conventional component C-4

Figure 7 shows the results of 3D scanning of component C-4 at various stages of processing and after initial operational loading. After conventional manufacturing, the surface is significantly uneven, with numerous deviations shown in purple tones. Heat treatment further accentuates these differences, as evidenced by the presence of large areas with high deviations. Subsequent machining significantly unifies the surface and eliminates most of the unevenness, as can be seen in the predominant blue and green areas. After coating, the surface remains uniform with minimal local changes. After 16,000 cycles, the first signs of wear appear, but the surface remains largely stable.

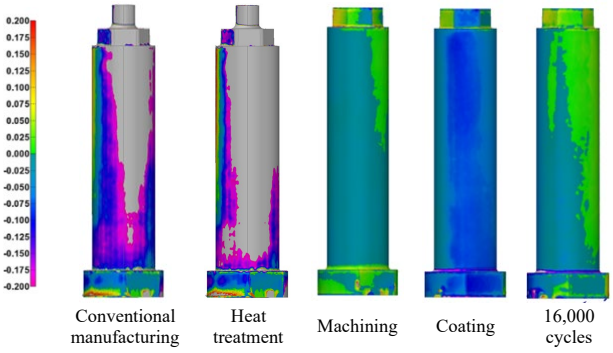


Fig. 7. First part of the technological process of component C-4

Figure 8 shows the results of 3D scanning of the sample surface after gradual loading during its life cycle.

After 32,000 cycles, the surface is relatively homogeneous with minor local changes, which are mainly visible at the bottom of the component. After 78,000 cycles, wear spreads but remains at an acceptable level, and the surface does not show any significant degradation. At 97,000 cycles, larger areas with yellow tones appear, indicating a more significant loss of material and an increase in unevenness. After 103,400 cycles, these areas continue to expand and the surface begins to become noticeably uneven. After reaching 115,500 cycles, significant surface degradation with greater deviations is evident, especially in the upper part of the component, which confirms the gradual deterioration of surface properties under long-term operational loading.

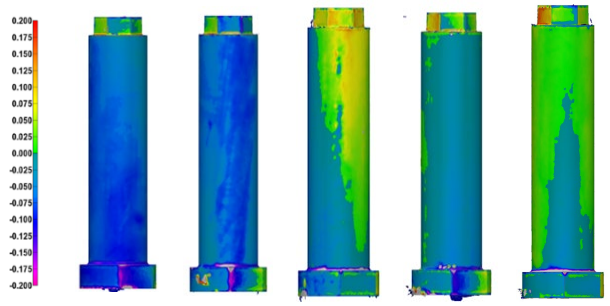


Fig. 8. Second part of the technological process of component C-4

Scanning of the additive component 3D-3

Figure 9 shows the results of 3D scanning of the sample after coating and subsequent loading at various stages of the operating cycle.

Immediately after coating, significant surface unevenness is apparent, especially in the upper part of the component. After 16,000 loading cycles, the surface becomes significantly more even and most of the area stabilises. This condition is maintained even after 32,000 cycles, when the surface is still uniform and shows no major signs of wear. Even after 78,000 cycles, no significant degradation is observed, and the surface remains largely homogeneous with minor local deviations, indicating good coating stability under long-term loading.

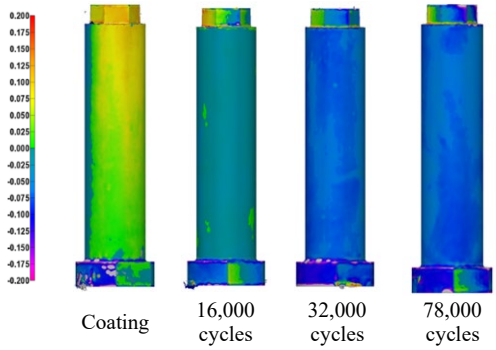


Fig. 9. First part of the technological process of component 3D-3

Figure 10 shows the development of the sample surface after long-term loading, after 97,000, 103,400, and 115,500 cycles. After 97,000 cycles, the surface is still largely uniform. After 103,400 cycles, these areas expand further and the surface becomes

more uneven, indicating accelerating material degradation. After reaching 115,500 cycles, the surface is significantly damaged, indicating a change in surface geometry.

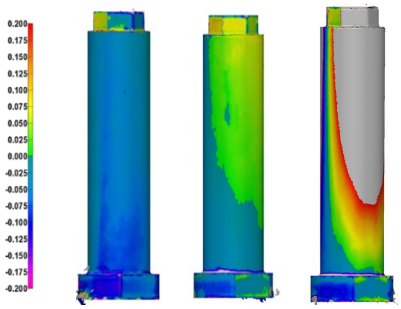


Fig. 10. Second part of the technological process of component 3D-3

Scanning of additive component 3D-4

Figure 11 shows the results of 3D scanning of the sample surface after coating and subsequent loading at different numbers of cycles.

Immediately after coating, the surface is predominantly homogeneous, with minor local deviations. After 16,000 cycles, the surface still appears stable, with blue tones predominating and no significant changes apparent. However, after 32,000 cycles, extensive areas of red and grey tones appear, indicating significant surface wear and degradation, especially in the upper part of the sample. After 78,000 cycles, the damage spreads further and green-yellow areas confirm significant surface unevenness, indicating continued material degradation under long-term loading.

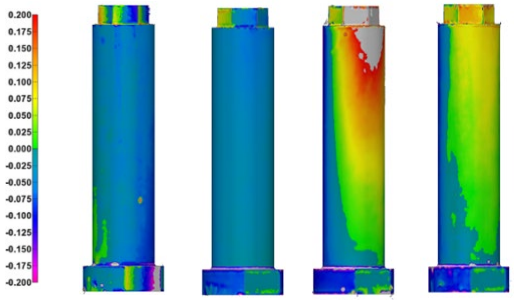


Fig. 11. First part of the technological process of component 3D-4

Figure 12 shows the results of 3D scanning of the sample surface after long-term loading, after 97,000, 103,400, and 115,500 cycles.

After 97,000 cycles, the surface is still relatively uniform, with blue tones predominating and only localised signs of significant wear. After 103,400 cycles, however, an extensive area appears that shows advanced surface degradation. After reaching 115,500 cycles, the damage spreads further, and a distinct red and grey area at the top of the sample demonstrates changes in surface geometry. This condition can be considered the final stage of the sample's service life.

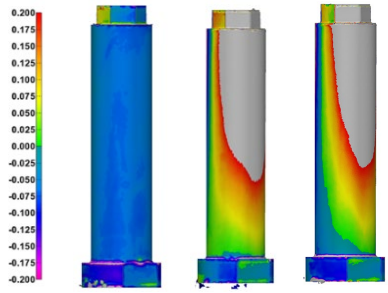


Fig. 12. Second part of the technological process of component 3D-4

3.1. Porosity

The measurement methods also included an assessment of micro-porosity in conventionally and additively manufactured components due to its impact on the mechanical properties of the material and the dimensional accuracy of the components. An example of porosity distribution in conventional and additive components is shown in Figure 13.

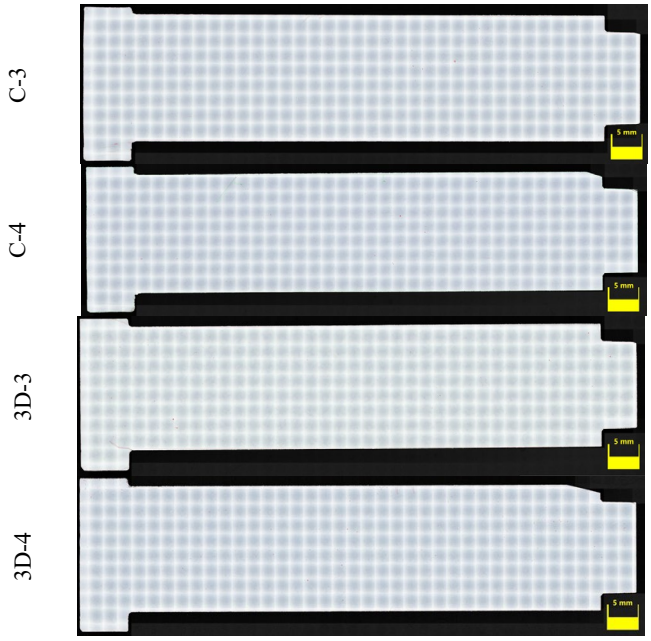


Fig. 13. Porosity distribution in conventionally and additively manufactured H13 components.

Table 4 shows the porosity values of all evaluated components. A porosity volume of 0.04 and 0.03% was measured in both conventional and additive components.

Table 4.
Porosity of the conventional and 3D printed H13 samples

Conventional samples	Porosity (%)	**3D printed samples**	Porosity (%)
C-3	0.04	**3D-3**	0.03
C-4	0.03	**3D-4**	0.04

3.2. Roughness measurement on the surface of the component crown using a confocal light microscope

The red arrows in Figure 14 indicate specific areas on the crown where surface roughness measurements were taken. These locations were selected to represent the character of the surface created during the manufacturing process and to enable evaluation of the quality of machining or follow-up surface treatment and subsequent operational wear. The location of the measuring points on the crown ensures sufficiently accurate and repeatable results, which can then be compared with the hardness values or other mechanical properties determined on the same sample.

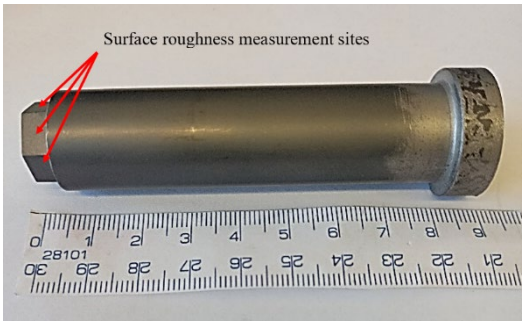


Fig. 14. Roughness measurement locations

Figure 15 shows a colour map of the surface obtained using a confocal microscope, which captures the topography of the examined area. The colour scale on the right shows the height differences of the surface, from the lower parts in tones of blue to the highest peaks in red. The area is marked with arrows and numbered areas where detailed roughness measurements were performed. These locations were chosen to represent different characteristic parts of the surface and to provide the most accurate picture of its actual morphology.

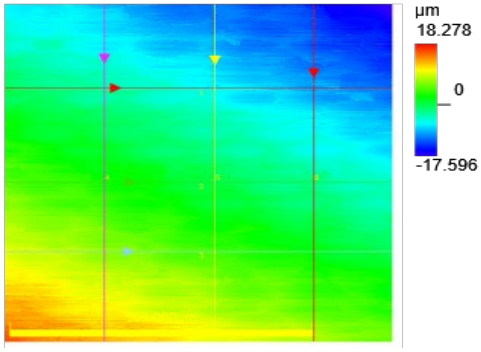


Fig. 15. Surface topography obtained using confocal microscopy

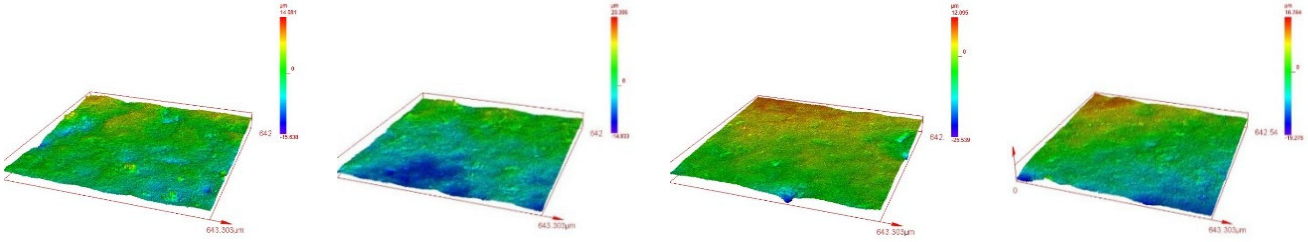
The results of roughness measurements from both measurement directions are summarised in Table 5.

Table 5.
Measured roughness values

Component designation	Ra [µm]
C-3	1.28 ± 0.24
C-4	1.56 ± 0.21
3D-3	1.56 ±0.64
3D-4	0.87 ± 0.20

Measurement of roughness of components C-3, C-4, 3D-3 and 3D-4

Figure 16 a–d show the 3D topography of the surface of the analysed components (C-3, C-4, 3D-3, and 3D-4) obtained using confocal microscopy. The colour scale expresses surface height differences from approximately −25 µm to +20 µm, depending on the specific sample. The average arithmetic roughness Ra reached values of 1.28 ± 0.24 µm for component C-3, 1.56 ± 0.21 µm for C-4, 1.56 ± 0.64 µm for 3D-3, and 0.87 ± 0.20 µm for 3D-4.


a) 3D visualisation of the roughness of component C-3

b) 3D visualisation of the roughness of component C-4

c) 3D visualisation of the roughness of component 3D-3

d) 3D visualisation of the roughness of component 3D-4

Fig. 16. Visualisation of component roughness

Conventionally manufactured components (C-3 and C-4) exhibited comparable levels of roughness, while additive component 3D-3 was characterised by greater surface variability, as evidenced by a larger standard deviation. In contrast, component 3D-4 achieved the lowest Ra value and also exhibited a more homogeneous topography. Overall, the roughness of all evaluated surfaces ranged from 0.87 to 1.56 µm, with no pronounced extremes in surface morphology.

Vickers hardness measurement

Measuring points numbered 1 to 10 were marked on the surface of the mounted and ground sample, as shown in Figure 17. Hardness testing was performed at these points using the Vickers method (HV10). The data obtained in this way was then converted into graphs showing the hardness curve from point 1 to point 10.

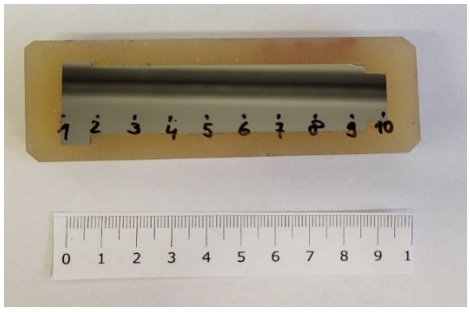


Fig. 17. View of the mounted and ground sample for hardness measurement

Measurement of hardness of component C-3

Figure 18 shows the hardness profile of component C-3 along its axis. At the beginning of the measurement (points 1–3), the hardness values are around 300 HV10 and show only a slight increase. From point 3 to point 4, there is a sharp increase in hardness from approximately 320 HV10 to more than 400 HV10. Subsequently, between points 4–6, the hardness continues to rise, but less significantly, and stabilises around 450 HV10. From point 6 to the end of the measurement (points 7–10), the hardness values remain relatively stable, with only minor fluctuations around 450 HV10. Overall, it is clear that the hardness along the axis increases gradually at the first measured points, then increases sharply and finally stabilises at a higher stable level. The lower hardness in the initial region and the subsequent increase may reflect local variations in thermal history; however, confirmation of the underlying cause would require direct microstructural analysis.

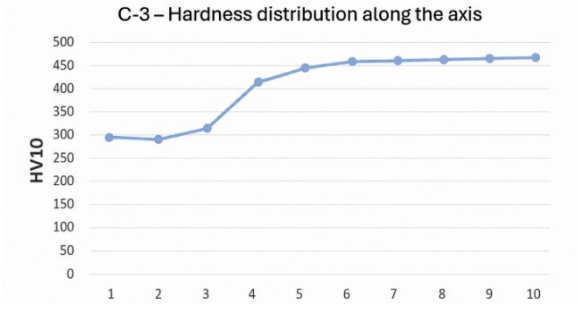


Fig. 18. Hardness development in component C-3

Hardness measurement of component C-4

Figure 19 shows the hardness profile of component C-4 along its axis. At the first three measurement points, the hardness is around 300 HV10, with a slight decrease below this value between points 2 and 3. However, from point 3 to point 4, there is a sudden increase in hardness to more than 430 HV10. From this point on, the hardness stabilises and remains at a constant level of around 440–450 HV10 for the remaining measurements (points 4–10), with minimal fluctuation. This observation indicates that the initial region of the sample exhibits lower hardness. The subsequent increase and stabilisation from point 4 onwards may reflect local variations in thermal history or heat-treatment response; however, confirmation of the underlying cause would require direct microstructural analysis.

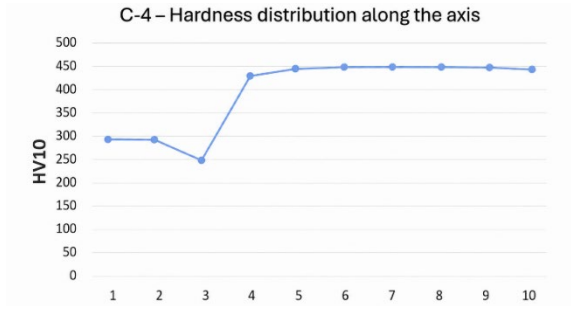


Fig. 19. Hardness development in component C-4

Hardness measurement of component 3D-3

Figure 20 shows the hardness profile of component 3D-3 along its axis. The hardness at all the measured points falls within a narrow range of approximately 492–502 HV10. At the beginning (points 1–3), the values are very stable at around 499–500 HV10. Subsequently, at points 4 and 5, there are minor fluctuations, but the values remain close to 500 HV10. From point 6, the hardness decreases slightly and reaches a minimum of approximately 492 HV10 around point 9. At the last measured point (10), however, it rises sharply again and returns to a level around 501 HV10. Overall, the hardness of component 3D-3 was relatively uniform along the measured axis, with only minor local fluctuations. This trend indicates a relatively uniform hardness distribution and stable mechanical response.

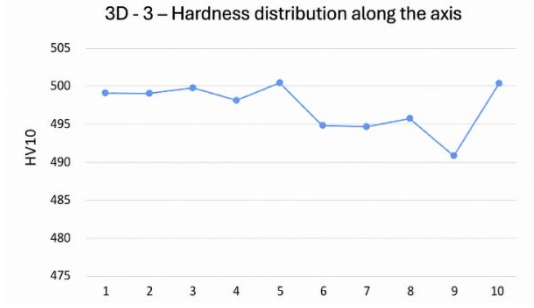


Fig. 20. Hardness development in component 3D-3

Hardness measurement of component 3D-4

Figure 21 shows the hardness profile of component 3D-4 along its axis. The hardness ranges from approximately 481 to 495 HV10. At the beginning (point 1), the value is higher, around 495 HV10; then there is a slight decrease, and between points 2–5, the hardness remains stable at around 489–491 HV10. At point 6, the value increases slightly again, but from point 7 it gradually decreases to a minimum of around 481 HV10 at point 9. At the final point (10), there is a partial compensation, and the hardness returns to a value of around 490 HV10. Overall, the hardness of sample 3D-4 was relatively uniform along the measured axis, although minor

fluctuations and a gradual decrease towards point 9 were observed. These variations may reflect local differences in thermal history or heat-treatment response; however, confirmation of their origin would require direct microstructural analysis.

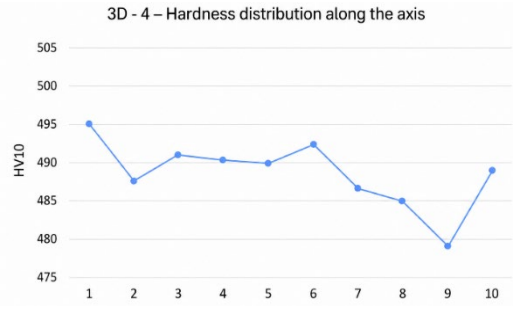


Fig. 21. Hardness development in component 3D-4

4. Conclusions

In this study, the properties of conventionally manufactured and additively manufactured H13 tool steel components were compared under operating conditions in a die-casting foundry. The results show that porosity was very low for both technologies (0.03–0.04%), which was achieved through using appropriately selected manufacturing parameters.

Surface roughness measurements showed that the conventionally manufactured components exhibited Ra values ranging from 1.28 to 1.56 µm, whereas the additively manufactured components exhibited Ra values ranging from 0.87 to 1.56 µm. Sample 3D-3 showed the greatest roughness variability, whereas sample 3D-4 exhibited the lowest mean Ra value.

The hardness of conventional components after heat treatment reached values around 450 HV, while additive components exhibited higher and more stable hardness levels in the range of 481–502 HV. Differences in hardness distribution along the sample axes may reflect variations in thermal history or heat-treatment response; however, their underlying causes cannot be confirmed without direct microstructural analysis.

All four components completed 115,500 casting cycles under operational foundry conditions. However, surface analyses revealed gradual wear, which manifested at different rates and to varying degrees in individual samples depending on the manufacturing technology used and subsequent treatments.

Both component types remained operational throughout the test. Although differences in surface roughness and post-service hardness distribution were observed, the results indicate that SLM represents a promising alternative for the production of H13 tooling components used under demanding high-pressure die-casting conditions.

Acknowledgements

The paper was funded the Technology Agency of the Czech Republic within the scope of the TREND program. as part of projects Reg. No. FW03010609 “Research and development of shape molds made of H-13 and DIEVAR for die casting of aluminum alloys in the application of modern technologies of additive production. heat treatment. surface treatment and numerical simulations”.

This research was supported by the Ministry of Education, Youth and Sports of the Czech Republic within the Specific University Research programme (project no. 05SVV2026p2 “Integration of advanced technologies, AI and public participation in applied research”).

References

[1] Lei, F., Wen, T., Yang, F., Wang, J., Fu, J., Yang, H., Wang, J., Ruan, J. & Ji, S. (2022). Microstructures and mechanical properties of H13 tool steel fabricated by selective laser melting. *Materials*. 15(7), 2686, 1-15. DOI: 10.3390/ma15072686.

[2] Günen, A., Heidarzadeh, A., Ceritbinmez, F., Kanca, E., Li, W. & Çam, G. (2026). Drilling response of additively manufactured and cast AlSi H13 hot-work tool steel by thermal and mechanical processes. *Progress in Additive Manufacturing*. 11(1), 157-179. DOI: 10.1007/s40964-025-01340-w.

[3] Huang, G., Wei, K. & Zeng, X. (2022). Microstructure and mechanical properties of H13 tool steel fabricated by high power laser powder bed fusion. *Materials Science and Engineering A*. 858, 144154, 1-10. DOI: 10.1016/j.msea.2022.144154.

[4] Wu, L., Das, S., Gridin, W., Leuders, S., Kahlert, M., Vollmer, M. & Niendorf, T. (2021). Hot work tool steel processed by laser powder bed fusion: a review on most relevant influencing factors. *Advanced Engineering Materials*. 23(7), 2100049, 1-29. DOI: 10.1002/adem.202100049.

[5] Miyauchi, H., Matsumoto, H. & Yokota, K. (2022). Selective laser melting with changing input energy periodically for production of partially hardened laminate structure in H13 steel. *Journal of Manufacturing Processes*. 73(2), 839-848. DOI: 10.1016/j.jmapro.2021.11.028.

[6] Kim, Y.W., Park, H., Eom, Y.S., Ahn, D.G., Kim, K.T., Yu, J.H., Choi, Y.S. & Park, J.M. (2023). High-speed manufacturing-driven strength-ductility improvement of H13 tool steel fabricated by selective laser melting. *Powder Metallurgy*. 66(5), 582-592. DOI: 10.1080/00325899.2023.2241245.

[7] Karakas, M.S., Günen, A., Lindner, T., Küçük, Y., Kon, Ö., Joshi, S., Çam, G. & Lampke, T. (2025). Comparative study of heat treatment routes for enhancing high-temperature wear resistance of EBM-processed Inconel 718. *Materials Today Communications*. 49, 113864, 1-16. https://doi.org/10.1016/j.mtcomm.2025.113864.

[8] Günen, A., Gürol, U., Çakan, A., Koçak, M., Çam, G., Yildizhan, H., Alsaadi, A. & Gomes, J. (2025). Effect of post-deposition aluminizing on the corrosion and mechanical behavior of WAAM-fabricated stainless steel and Ni-based superalloy. *Scientific Reports*. 15, 43268, 1-17. DOI: 10.1038/s41598-025-30389-4.

[9] Kocaman, E., Gürol, U., Günen, A. & Çam, G. (2025). Effect of post-deposition heat treatments on high-temperature wear

and corrosion behavior of Inconel 625. *Materials Today Communications*. 42, 111101, 1-17. DOI: 10.1016/j.mtcomm.2024.111101.
[10] Cam, G. & Gunen, A. (2024). Challenges and opportunities in the production of magnesium parts by directed energy deposition processes. *Journal of Magnesium and Alloys*. 12(5), 1663-1686. DOI: 10.1016/j.jma.2024.05.004.
[11] Impaziente, F., Giorleo, L. & Mazzucato, F. (2024). Selective laser melting of H13 tool steel powder: effect of process parameter on complex part production. *Progress in Additive Manufacturing*. 9(4), 1071-1084. https://doi.org/10.1007/s40964-023-00504-w.
[12] Katancik, M., Mirzababaei, S., Ghayoor, M. & Pasebani, S. (2020). Selective laser melting and tempering of H13 tool steel for rapid tooling applications. *Journal of Alloys and Compounds*. 849, 156319, 1-12. DOI: 10.1016/j.jallcom.2020.156319.
[13] Santhoshsarang, D.M., Narayanaswamy, S., Telasang, G., Divya, K., Bathe, R. & Samuel, G.L. (2025). Additive Manufacturing of AISI H13 Tool Steel with Combinations of Higher Laser Power and Scan Speed: Microstructural and Mechanical Properties Insights. *Journal of Materials Engineering and Performance*. 34, 17491-17502. DOI: 10.1007/s11665-024-10467-w.
[14] Monjez, M.M., Omidi, N., Farhadipour, P., Barka, N. & El Ouafi, A. (2025). Process-structure–property relationships in laser powder bed fusion of H13 tool steel: effect of processing and tempering conditions on microstructure and mechanical properties. *The International Journal of Advanced Manufacturing Technology*. 139, 2481-2504. DOI: 10.1007/s00170-025-14174-y.
[15] Baali, L., Dehghan, S., Iltaf, A., Barka, N. & Dassylva-Raymond, V. (2024). Experimental and statistical study on mechanical behavior of H13 tool steel additively manufactured and laser surface treated. *Lasers in Manufacturing and Materials Processing*. 11(2), 193-217. DOI: 10.1007/s40516-023-00239-0.
[16] Hosseinlou, H., Shakeri, M., Abdelghany, A.W. & Jaskari, M. (2025). Tailoring microstructure and mechanical properties of additively manufactured H13 tool steel: influence of build orientation and tempering treatments. *Materials Science and Engineering A*. 942, 148708, 1-17. DOI: 10.1016/j.msea.2025.148708.
[17] Bae, K., Moon, H. S., Park, Y., Jo, I. & Lee, J. (2022). Influence of tempering temperature and time on microstructure and mechanical properties of additively manufactured H13 tool steel. *Materials*. 15(23), 8329, 1-10. https://doi.org/10.3390/ma15238329.
[18] Cui, C., Wang, D., Hao, Z., Wang, P., Ma, R. & Shu, Y. (2025). Laser powder bed fusion of H13 tool steel with tungsten-lanthanum oxide particles addition. *Materials Research Letters*. 20(1), e2499928, 1-15. DOI: 10.1080/17452759.2025.2499928.
[19] Qin, Z., Kang, N. & El Mansori, M. (2024). Surface condition driven fatigue performance of laser powder bed fusion H13 steel. *Journal of Materials Research and Technology*. 33, 6767-6779. DOI: 10.1016/j.jmrt.2024.11.048.
[20] Zong, H., Kang, N. & El Mansori, M. (2024). Impact of applied loads on wear mechanisms in H13 steel at various preheating temperatures during laser powder bed fusion additive manufacturing. *Wear*. 556-557, 205538, 1-14. DOI: 10.1016/j.wear.2024.205538.
[21] Fonseca, E.B., Gabriel, A.H., Ávila, J.A., Vaz, R.F., Valim, D. B., Cano, I. G. & Lopes, É. S. (2023). Fracture toughness and wear resistance of heat treated H13 tool steel processed by laser powder bed fusion. *Additive Manufacturing*. 78, 103862, 1-17. DOI: 10.1016/j.addma.2023.103862.
[22] Chang, C., Yan, X., Deng, Z., Lu, B., Bolot, R., Gardan, J., Deng, S., Chemkhi, M., Liu, M. & Liao, H. (2022). Heat treatment induced microstructural evolution, oxidation behavior and tribological properties of Fe-12Cr-9Ni-2Al steel (CX steel) prepared using selective laser melting. *Surface and Coatings Technology*. 429, 127982, 1-15. DOI: 10.1016/j.surfcoat.2021.127982.
[23] Girisken, I. & Cam, G. (2023). Characterization of microstructure and high-temperature wear behavior of pack-borided Co-based Haynes 25 superalloy. *CIRP Journal of Manufacturing Science and Technology*. 45, 82-98. DOI: 10.1016/j.cirpj.2023.06.012.
[24] Günen, A., Gürol, U., Koçak, M. & Çam, G. (2023). Investigation into the influence of boronizing on the wear behavior of additively manufactured Inconel 625 alloy at elevated temperature. *Progress in Additive Manufacturing*. 8(6), 1281-1301. DOI: 10.1007/s40964-023-00398-8.
[25] Günen, A., Gürol, U., Koçak, M. & Çam, G. (2023). A new approach to improve some properties of wire arc additively manufactured stainless steel components: Simultaneous homogenization and boriding. *Surface and Coatings Technology*. 460, 129395, 1-18. DOI: 10.1016/j.surfcoat.2023.129395.
[26] Chantziara, K., Nikas, D., Bergström, J., Grehk, M., Pappa, M. & Michailidis, N. (2024). High and very high cycle fatigue behaviour of additively manufactured H13 hot work tool steel. *Materials Science and Engineering A*. 890, 146958, 1-16. https://doi.org/10.1016/j.msea.2024.147401.
[27] Kuriachen, B., Vinay, K. & Joshy, J. (2024). Influence of post-processing and build direction on the wear behavior of laser powder bed fused maraging steel. *Journal of Tribology*. 146(10), 104201. DOI: 10.1115/1.4065499.
[28] Narvan, M., Al-Rubaie, K.S. & Elbestawi, M. (2019). Process-structure-property relationships of AISI H13 tool steel processed with selective laser melting. *Materials*. 12(14), 2284, 1-20. DOI: 10.3390/ma12142284.
[29] Han, L., Wang, Y., Zhang, Z. & Liu, S. (2024). Assessment of mechanical behavior in H13 tool steel synthesized through electron beam melting and selective laser melting techniques. *Steel Research International*. 95(8), e202300827, 1-10. DOI: 10.1002/srin.202300827.
[30] Sun, Y., Wang, J., Li, M., Wang, Y., Li, C., Dai, T., Hao, M. & Ding, H. (2022). Thermal and mechanical properties of selective laser melted and heat treated H13 hot work tool steel. *Materials & Design*. 224, 111295, 1-13. DOI: 10.1016/j.matdes.2022.111295.
[31] Omidi, N., Farhadipour, P., Baali, L., Bensalem, K., Barka, N. & Jahazi, M. (2023). A comprehensive review of additively manufactured H13 tool steel applicable in the injection mold industry. *JOM*. 75(11), 4457-4469. https://doi.org/10.1007/s11837-023-05735-4.